

# NUMERICAL SIMULATION OF REINFORCED CONCRETE SHEAR WALL USING 3D-NLFEA

Ainun Najib<sup>a</sup>, Bambang Piscea<sup>b\*</sup>, Harun Alrasyid<sup>b</sup>

**Abstract:** This paper present a numerical simulation of a reinforced concrete shear wall loaded under in-plane and out-of-plane directions using a 3D-NLFEA finite element package. The applied vertical load is controlled as a fraction of the horizontal in-plane load. Therefore, inside the 3D-NLFEA package, a special routine was developed to account for changes in the vertical load as a function of the lateral load. The performance of the numerical model is evaluated by comparing not only the load-deformation response but also the normalized average strain along the length and height of the shear wall. This study found that the predicted peak and ultimate load only differ by about 0.5% and 0.4%, respectively. By observing the location where the normalized average strain is zero, the average compressive stress from the numerical model can be back-calculated and is 39.73 MPa which is higher than the unconfined concrete compressive strength due to confinement to the core by the tie in the boundary element. On the other hand, the back-calculated average compressive stress from the test result is 26.11 MPa which is lower than the unconfined concrete compressive strength. Therefore, it can be concluded that the proposed numerical model for predicting the shear behavior loaded under in-plane and out-of-plane directions were found to be reasonable and satisfactory.

**Keywords:** Shear walls, three-dimensional finite element method, out-of-plane instability, high-rise buildings, reinforced concrete

Submitted: 12 August 2021; Revised: 22 December 2022; Accepted: 22 December 2022

## INTRODUCTION

Reinforced concrete (RC) shear walls have been widely used in high-rise buildings. In areas with high seismic zones, a structure must have sufficient ductility to withstand the forces that occur during the seismic event. In design with the dual-system concept, the shear walls should resist a maximum of 75% of the seismic force. The rest of the shear forces should be carried out by the structural frame. Therefore, during the seismic event, RC shear wall should be well-designed to avoid brittle failure and maintain the integrity of the whole. The RC shear wall must be designed to carry the load in a three-dimensional state.

The load that acts on the RC shear wall is mainly in the in-plane direction. Some other forces are the shear force in the out-of-plane and axial directions. For a slender shear wall, the out-of-plane force can increase the P-Delta effect and, along with the axial force acting on the shear wall cross-section, will increase the 2<sup>nd</sup> order bending moment and may produce buckling of both the shear wall and reinforcing bar in the compression zone [1], [2].

In the high-compressive region, the possible failure can be classified as buckling of the compression reinforcement, crushing of the concrete core due to inadequate restraint, and lateral geometric instability, also known as out-of-plane buckling. To study the non-linear behavior of RC shear walls with complex states of loadings, the 3D-NLFEA package, which utilizes the plasticity-fracture model and customized loading condition, is used. The proposed numerical simulation is verified by comparing the available test result in the literature [3]. The study presented not only the load-deformation curve but also the crack pattern and the load strain distribution along the height and the length of the shear wall.

## RESEARCH SIGNIFICANCE

This paper investigates the non-linear behavior of RC shear walls loaded under in-plane and out-of-plane directions using the 3D-NLFEA package. The bending moment from the upper story was accounted into the model using a custom loading function incorporated inside the 3D-NLFEA package. This custom loading function updates the axial force in the accumulator beam as a function of the applied horizontal forces. It is balanced during the global non-linear iteration for each sub-step to maintain the global equilibrium of the forces.

## METHODOLOGY

### A. GEOMETRY OF THE SHEAR WALLS AND BOUNDARY CONDITIONS

Figure 1 shows the side and front views geometry of the shear walls which was generated from the available information in the literature [3]. The hatched region (inclined line) in Figure 1 is the accumulator beam that is set to be rigid to mimic the experimental test setup. The in-plane force or displacement direction is noted as  $H_x$  in Figure 1 and is placed on the long accumulator beam (the cross-sectional size of the accumulator beam is 500 mm × 500 mm). The force  $H_x$  is located at the mid-height of the long accumulator beam such that it would allow rotation in the long accumulator beam. The axial force that acts at the shear wall's top is applied by half of the axial force ( $P/2$ ) at the left and right of the shear wall in the longitudinal direction. Notice that in Figure 1, in addition to  $P/2$  as the axial force, there exist  $\Delta V_1$  and  $\Delta V_2$ , which have opposite directions. These variables  $\Delta V_1$  and  $\Delta V_2$  are to accommodate the changes in the axial force due to the presence of bending moment from the upper story level and are a function of the force  $H_x$ . The level arm for  $\Delta V_1$  and  $\Delta V_2$  is 4600 mm. The out-of-plane load is applied via the side accumulator beam and is noted as  $H_y$  in Figure 1. The side accumulator beam has a cross-sectional size of 300 mm x 600 mm.

<sup>a</sup>Master Student in the Civil Engineering Department, Institut Teknologi Sepuluh Nopember, ITS Campus, Sukolilo, Surabaya 60111, Indonesia.

<sup>b</sup>Lecturer in the Civil Engineering Department, Institut Teknologi Sepuluh Nopember, ITS Campus, Sukolilo, Surabaya 60111, Indonesia. Corresponding author email address: piscesa@ce.its.ac.id

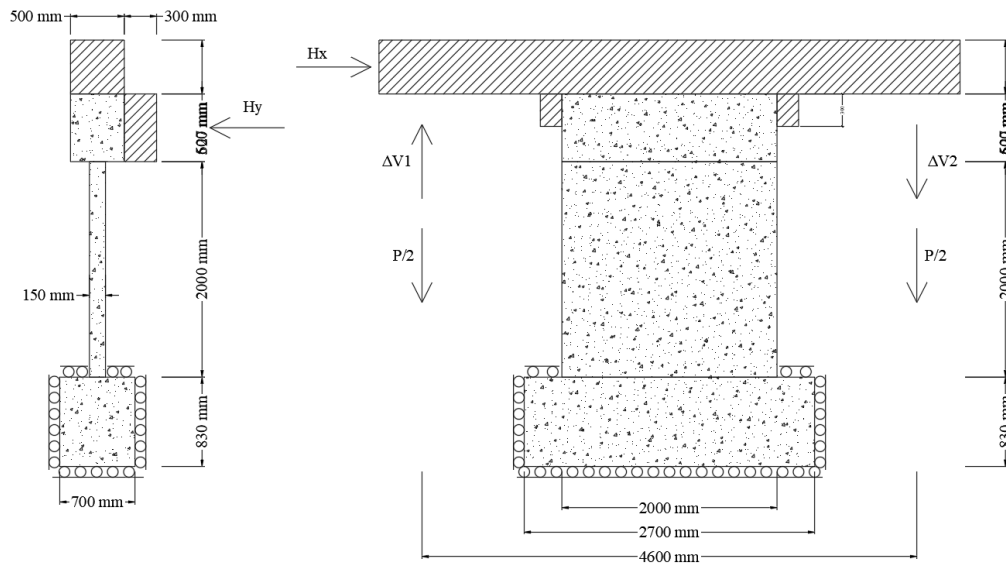


Figure 1 Shear wall geometry and load set-up test

Table 1 Load and drift comparisons between the 3D-NLFEA prediction and test result

Stage	Lateral Load (kN)			Lateral Drift (%)		
	Exp.	Model	Ratio Exp./Model	Exp.	Model	Ratio Exp./Model
Yielding	243.36	242.07	1.005	0.37	0.34	1.107
Ultimate	251.62	252.58	0.996	2.07	1.96	1.054

Figure 1 also shows the boundary condition of the shear wall where the bottom stub is fixed in the orthogonal direction for each side (roller). By assuming this condition, the support for the RC shear wall behaves as if the bottom stub were well anchored to the strong floor. The tested shear wall has a thickness of 150 mm, a length of 2000 mm, and a height of 2000 mm. The top stub has a dimension of 500 mm x 600 mm x 2000 mm, while the bottom stub has a size of 700 mm x 830 mm x 2700 mm. The geometry was meshed using eight-node hexahedral elements with a mesh size of 50 mm.

## B. MATERIAL PROPERTIES AND CONSTITUTIVE MODELS

The concrete compressive strength of the shear wall is 35.94 MPa, and the elastic modulus is 28176 MPa. The Poisson's ratio of the concrete was set to 0.2. The assigned concrete constitutive model was the multi-surface plasticity model, which combines the compressive failure surface (Menetrey and Willam failure surface [4]) with the tension cut-off failure surface [5], [6]. The constitutive model for concrete under compression has a non-associative flow rule [7-10] while for concrete under tension follows the associative flow rule [11]. The concrete element is modeled as eight-node hexahedral element with BBar element technology [12].

The yield strength for the boundary condition reinforcement is 307 MPa, while the yield strength for the web reinforcement is 258 MPa. The constitutive model for the rebar was unsymmetric, which explains that the rebar behaves differently under compression or tension. When under tension, the bar behavior is set to a bilinear elastic-perfectly plastic model without hardening. On the other hand, when under compression, the bar behavior is elastic up to the yielding point and slowly softens due to buckling.

Figure 1 shows the stress-strain model for reinforcing bars with unsymmetric behavior. In Figure 1, the stress strain for the bar under tension (shown as a solid red line) has a bilinear shape.

On the other hand, the stress strain for the bar under compression (shown as a solid blue line) has a trilinear model without yielding a plateau to model the buckling of the bar under compression. In 3D-NLFEA, the reinforcing bar is modeled as a truss element and is embedded inside the parent element [13]. An iso-parametric formulation to relate the displacement of the bar with the movement of the parent element was used.

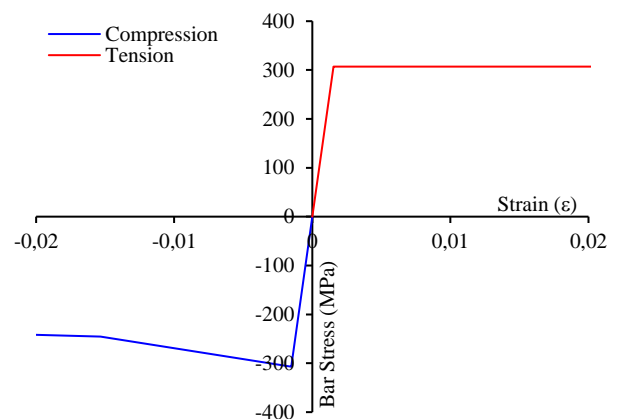


Figure 1 Stress-strain model for reinforcing bar

## C. LOADING METHODS

The modeled RC shear wall is laterally loaded in-plane and out-of-plane directions. The lateral load was obtained from the restraint force from the displacement control, which maintained a constant aspect ratio between the in-plane and out-of-plane directions. In the final step, the lateral

displacement in the in-plane direction is set to 60 mm, while the lateral displacement in the out-of-plane direction is set to 11 mm. The initial vertical load was given about 5.5% of the shear wall's axial load capacity, which was computed considering only the capacity of the concrete under compression. Initially, the vertical load (P) is distributed evenly via the accumulator beam and divided equally by P/2 in the vertical jack location. As the lateral displacement is given, the change in the vertical load is controlled as a portion of the exerted load from the lateral displacement control.

Hence, it can be written that the changes in the vertical load ( $\Delta V_1/\Delta V_2$ ) as:

$$\Delta V_1 = + \frac{H_u L_w}{H_w} \quad \text{and} \quad \Delta V_2 = - \frac{H_u L_w}{H_w} \quad (1)$$

In Eqn.(1),  $H_u$  is the exerted lateral force from the applied horizontal displacement,  $L_w$  is the length of the shear wall, and  $H_w$  is the height of the shear wall. During the global non-linear iteration, the equilibrium is maintained while adjusting the change in the vertical load as a function of the applied lateral force.

## ANALYSIS AND DISCUSSIONS

### A. LOAD-DISPLACEMENT CURVE

Figure 2 shows the load-displacement curve comparisons for shear wall SWD1 between the proposed model and the test result. In Figure 2, the displacement is monitored at the accumulator beam centroid in the lateral direction. Since the applied load is displacement control, the reaction force exerted from the forced displacement is recorded and plotted as the applied load.

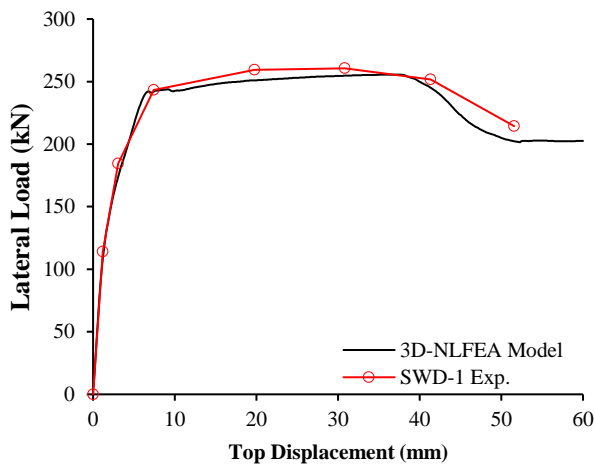


Figure 2 Load-displacement curve comparison

From Figure 2, it can be investigated that the model prediction was sufficiently accurate. The controlled vertical load as a function of the lateral force was found to be worked well. The load-displacement curve shown in Figure 2 can be distinguished into five stages: elastic, cracked, yielding, ultimate, and softened.

In the elastic stage, the stiffness between the numerical model and the tested specimen has similar behavior. After the concrete cracks, the 3D-NLFEA model barely has higher stiffness than the test result. At the yielding stage, the measured drift from the model is 0.34 % which is lower than the measured drift from the test result (0.37 %). At this

point, the measured lateral load capacity from the test result is 243.36 kN and from the model is 242.07 kN (0.50 % difference).

The ultimate stage of the shear wall is measured at the displacement point where the maximum lateral load capacity from the model was achieved, and the curve starts to soften. At this stage, the predicted maximum lateral load capacity is 252.58 kN which is higher than the test result (251.62 kN).

### B. CRACK PATTERN AND STRAIN LOCALIZATION

The strain localization was prepared using ParaView 5.9.0 [14], [15]. Figure 3 shows the crack pattern that occurred in the shear wall. The observed crack pattern was similar to the test result [3]. Figure 4 shows the strain distribution along the height of the shear wall. In Figure 3, it was clearly shown that the dark-colored region traveled from the outer or left side of the wall (tension region) to the right side (compression region). To support the evidence, the strain distribution along the height of the shear wall at the extreme tension side was also plotted in Figure 4. In Figure 4, the normalized average strain was investigated at several points along the height of the shear wall. One thing to note is that the normal strain is not similar to the test result data [3]. In the model, the localized crack occurred at a height between 0 to 300 mm from the bottom part of the shear wall. On the other hand, in the laboratory, the localized crack occurred from the bottom part of the shear wall up to a height of 630 mm. The normalized average strain from the model is 48, while the test result is 38.

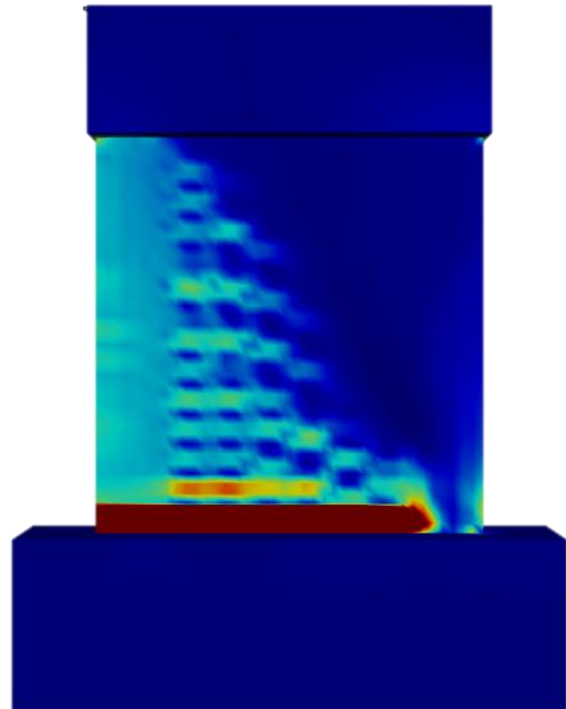


Figure 3 Crack pattern in the shear wall by observing the localized strain

Table 2 Load and drift comparisons between the 3D-NLFEA prediction and test result

Parameter	3D-NLFEA Model	Experiment
Length of the compression zone ( $L_w$ ) in mm	230	350
Confined concrete compressive strength ( $f'_{cc}$ ) in MPa	39.73	26.11
Ratio of $f'_{cc}/f'_c$	1.104	0.726

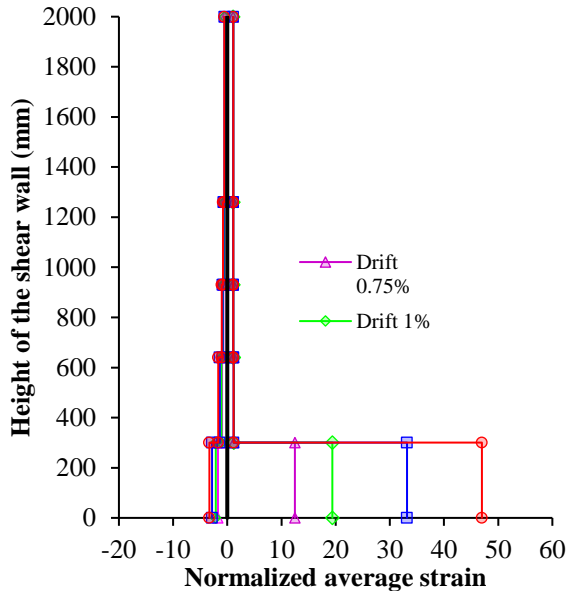


Figure 4 Normalized average strain along the height of the shear wall

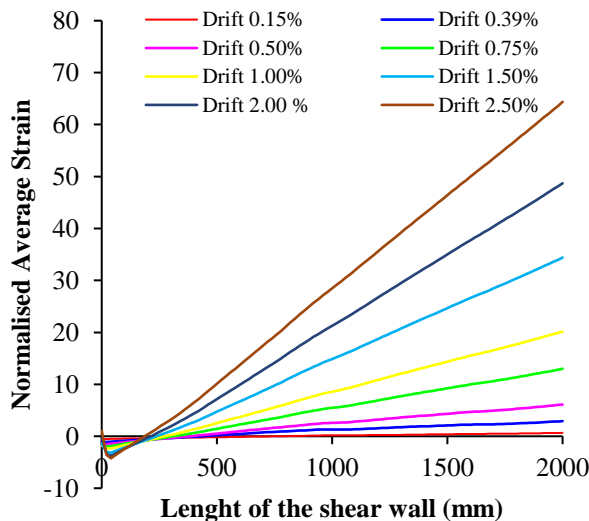


Figure 5 The normalized average strain distribution below the 300 mm height along the length of the shear wall

Figure 5 shows the strain distribution along the length of the shear wall. As shown in Figure 5, the strain distribution is almost linear from the compression to the tension side for each drift ratio. Up to a drift ratio of 0.38 %, the strain distribution was still symmetric between the compression and the tension sides. However, above that drift ratio, the strain is no longer symmetric but has a linear relationship. The average strain on the tension side at the ultimate stage is 0.0934. On the other hand, the average strain on the compression side is 0.007, far greater than the crushing strain of concrete, which is 0.003 for the unconfined

concrete. The portion of the unconfined concrete was already crushed, while for the confined concrete, as long as the confining bar did not yield, the confined compressive strength increased and thus may reduce the length of the compression area as the drift ratio increases.

### C. LENGTH OF COMPRESSION ZONE

The length of the compression zone at the level drift of 2.00 % can be seen in Figure 5 by looking at the distance of the zero strain from the outermost compression part. From Figure 5, the length of the compression zone is about 230 mm, while from the test result is about 350 mm. The differences between the numerical model and the test result might be caused by the restraint used in the model being more fixed than the test. To further check the compression zone length, the author uses a simple approach where only the tensile reinforcement is effectively resisting the tensile force at the boundary area. Thus, the tensile force can be computed as:

$$T = n \times A_s \times f_y = 10 \times 113 \times 307 = 346.8 \text{ kN} \quad (2)$$

By using the equilibrium of the forces acting on the shear wall cross-section, the tensile force contributed from the reinforcement is equal to the compressive force contributed from the concrete plus the applied normal force to the cross-section. Therefore, the length of the compression zone can be estimated as:

$$C = T + V = 346.8 \text{ kN} + 593.5 \text{ kN} = 940.3 \text{ kN} \quad (3)$$

$$L_w = \frac{C}{0.85 \times \beta_1 \times f'_c \times B'} \quad (4)$$

$$L_w = \frac{940300}{0.85 \times 0.807 \times 35.94 \times 150} = 254.3 \text{ mm} \quad (5)$$

From the calculation above, the compression zone's length is 254.3 mm. The length of the boundary condition is 300 mm and therefore has met the requirement for a special boundary element in ACI 318-19/SNI 2847-2019.

To compute the adjusted concrete compressive stress at the boundary element, one can back-calculate the average compressive stress by rearranging Eqn.(4) to get  $f'_c$  and maintain the concrete compressive block C. The notation B and  $\beta_1$  are the width of the shear wall and the equivalent factor of the concrete stress block. Table 2 shows the computed concrete compressive block for each length of the compression zone. From Table 2, the concrete compressive stress from the 3D-NLFEA model is 39.73 MPa which is higher than the unconfined concrete compressive strength expected due to confinement from the ties in the boundary element. On the other hand, the concrete compressive stress from the test result, which was back-calculated, is 26.11 MPa and is lower than the unconfined concrete strength.

## CONCLUSIONS

This paper briefly presents the numerical simulation of the RC shear wall using the 3D-NLFEA package. The proposed model was first verified with the available test result from the literature by looking at the global response of the applied lateral load as a function of the top lateral displacement. The error between the model and the test results in lateral load capacity at yield and ultimate was less than 0.5 percent.

The observation of the crack pattern, although only monotonic loading is considered, was similar to the one observed from the test result. However, from the normalized average strain along the shear wall height at the extreme tension fiber, the proposed model has a much larger value than the test result. The measured normalized average strain along the shear wall height from the model was 48 and from the test was 38 (the prediction from the model is about twenty-six percent higher than the test result).

The author also investigates the length of the compression zone by finding the value for the normalized average strain equal to zero. From the investigation, the length of the compression zone predicted by the model is 230 mm, while from the test result is 350 mm. Further investigation to back calculate the concrete compressive stress in the boundary element was also carried out. From the calculation, the predicted concrete compressive stress from the model is 39.73 MPa (higher than the unconfined concrete compressive strength) and from the test result is 26.11 MPa (lower than the unconfined concrete compressive strength).

## REFERENCES

- [1] J. W. Wallace *et al.*, "Damage and implications for seismic design of RC structural wall buildings," *Earthquake Spectra*, vol. 28, no. s1, pp. 281-299, 2012, doi: 10.1193/1.4000047.
- [2] C. W. Hilson, C. L. Segura, and J. W. Wallace, "Experimental study of longitudinal reinforcement buckling in reinforced concrete structural wall boundary elements," in *NCEE 2014 - 10th U.S. National Conference on Earthquake Engineering: Frontiers of Earthquake Engineering*, 2014, US-NCEE. doi: 10.4231/D3CC0TT9C.
- [3] M. Tripathi, R. P. Dhakal, and F. Dashti, "Bar buckling in ductile RC walls with different boundary zone detailing: Experimental investigation," *Engineering Structures*, vol. 198, 2019, doi: 10.1016/j.engstruct.2019.109544.
- [4] P. Menetrey and K. J. Willam, "Triaxial failure criterion for concrete and its generalization," *ACI Structural Journal*, vol. 92, no. 3, pp. 311-318, 1995.
- [5] B. Piscesa, M. M. Attard, D. Prasetya, and A. K. Samani, "Modeling cover spalling behavior in high strength reinforced concrete columns using a plasticity-fracture model," *Engineering Structures*, vol. 196, 2019, doi: 10.1016/j.engstruct.2019.109336.
- [6] J. Červenka and V. K. Papanikolaou, "Three dimensional combined fracture-plastic material model for concrete," *International Journal of Plasticity*, vol. 24, no. 12, pp. 2192-2220, 2008.
- [7] B. Piscesa, M. M. Attard, and A. K. Samani, "A lateral strain plasticity model for FRP confined concrete," *Composite Structures*, vol. 158, 2016. doi: 10.1016/j.compstruct.2016.09.028.
- [8] B. Piscesa, M. M. Attard, and A. K. Samani, "3D Finite element modeling of circular reinforced concrete columns confined with FRP using a plasticity based formulation," *Composite Structures*, vol. 194, 2018, doi: 10.1016/j.compstruct.2018.04.039.
- [9] B. Piscesa, M. M. Attard, and A. K. Samani, "Three-dimensional finite element analysis of circular reinforced concrete column confined with FRP using plasticity model," in *Procedia Engineering*, vol. 171, 2017, Elsevier. Ltd, doi: 10.1016/j.proeng.2017.01.377.
- [10] B. Piscesa, M. M. Attard, A. K. Samani, and S. Tangaramvong, "Plasticity constitutive model for stress-strain relationship of confined concrete," *ACI Structural Journal*, vol. 114, no. 2, pp. 361-371, 2017.
- [11] W.-F. Chen and D.-J. Han, *Plasticity for structural engineers*. J. Ross Publishing, 2007.
- [12] T. J. R. Hughes, *The finite element method: linear static and dynamic finite element analysis*. Courier Corporation, 2012.
- [13] A. Ranjbaran, "Mathematical formulation of embedded reinforcements in 3D brick elements," *Communications in Numerical Methods in Engineering*, vol. 12, no. 12, pp. 897-903, 1996.
- [14] U. Ayachit, *The paraview guide: a parallel visualization application*. Kitware Inc., 2015.
- [15] J. Ahrens, B. Geveci, and C. Law, *ParaView: An End-User Tool for Large-Data Visualization*. The Visualization Handbook, 2005.